Structure *14*, 477–485, March 2006 ©2006 Elsevier Ltd All rights reserved DOI 10.1016/j.str.2005.12.008

Structure and Dimerization of the Kinase Domain from Yeast Snf1, a Member of the Snf1/AMPK Protein Family

Vinod Nayak,[1,2] Kehao Zhao,[1] Anastasia Wyce,[1,3] Marc F. Schwartz,[1] Wan-Sheng Lo,[1] Shelley L. Berger,[1] and Ronen Marmorstein[1,2,*]
[1] The Wistar Institute
[2] Department of Chemistry
University of Pennsylvania
[3] University of Pennsylvania School of Medicine
Philadelphia, Pennsylvania 19104

Summary

The Snf1/AMPK kinases are intracellular energy sensors, and the AMPK pathway has been implicated in a variety of metabolic human disorders. Here we report the crystal structure of the kinase domain from yeast Snf1, revealing a bilobe kinase fold with greatest homology to cyclin-dependant kinase-2. Unexpectedly, the crystal structure also reveals a novel homodimer that we show also forms in solution, as demonstrated by equilibrium sedimentation, and in yeast cells, as shown by coimmunoprecipitation of differentially tagged intact Snf1. A mapping of sequence conservation suggests that dimer formation is a conserved feature of the Snf1/AMPK kinases. The conformation of the conserved αC helix, and the burial of the activation segment and substrate binding site within the dimer, suggests that it represents an inactive form of the kinase. Taken together, these studies suggest another layer of kinase regulation within the Snf1/AMPK family, and an avenue for development of AMPK-specific activating compounds.

Introduction

Members of the Snf1/AMP-activated kinase (AMPK) family are conserved in all eukaryotes and play fundamental roles in cellular responses to metabolic stress (Carling, 2004; Hardie et al., 1998). While mammals, insects, nematodes, and plants have multiple genes encoding AMPK homologs, yeast has only the one *SNF1* gene. Yeast Snf1 and mammalian AMPK are the most extensively studied members of this protein family. Multiple stress signals elevate the AMP-to-ATP ratio, which in turn results in the activation of AMPK to switch off ATP-consuming anabolic pathways and to switch on ATP-producing catabolic pathways. AMPK is also activated by leptin, a hormone that regulates food intake (Minokoshi et al., 2002), and metformin, a drug used to treat type-II diabetes (Zhou et al., 2001). In addition, mutations in the γ2 regulatory subunit of AMPK produce a cardiac disease in humans called Wolf-Parkinson syndrome (Arad et al., 2002), and LKB1, a target of inactivating mutations in a dominantly inherited cancer in humans termed Peutz-Jeghers syndrome, has been identified as an AMPK upstream kinase (Woods et al., 2003). Because of these correlations with disease, AMPK has received considerable attention as a possible target for the development of compounds that might regulate its activity for therapeutic application (Clapham, 2004).

In the yeast *Saccharomyces cerevisiae*, Snf1 (sucrose nonfermenting 1) is also required for stress responses and, most notably, the adaptation of cells to carbon stress (Sanz, 2003). For example, cells growing in high glucose maintain Snf1 in an inactive state. However, when the glucose levels are depleted, Snf1 is activated to regulate gene expression by phosphorylating several different transcriptional regulators. For example, Snf1 inhibits the transcriptional repressor Mig1 (Treitel, 1998), stimulates the transcriptional activators Cat8 and Sip4 (Hiesinger et al., 2001), and directly interacts with the Srb/mediator proteins of the RNA polymerase holoenzyme (Kuchin et al., 2000).

Other studies have revealed another aspect of Snf1 function during stress response. Snf1 has been shown to phosphorylate histone H3 in a promoter-specific fashion (Lo et al., 2001; Lo et al., 2005). On a subset of Gcn5-regulated promoters, such as the INO1, Snf1 phosphorylates serine 10 of histone H3 to promote subsequent acetylation of Lys14 by the Gcn5 histone acetyltransferase. In addition to histone phosphorylation and acetylation, histones have been shown to receive other posttranslational modifications, including methylation and ubiquitination (Ausio et al., 2001; Grant, 2001), and the process by which coordinated modifications, such as phosphorylation and acetylation leading to distinct transcriptional events, has been described as the "histone code" hypothesis (Strahl and Allis, 2000).

Genetic and biochemical studies have revealed that Snf1 is the catalytic (α) subunit of a trimeric protein complex, which, in addition to Snf1, contains one of the β subunits Sip1, Sip2, or Gal83, and the γ subunit Snf4 (Halford et al., 2004; Jiang and Carlson, 1997). Snf1 is a 633 amino acid protein with a kinase domain of about 330 residues, near the amino terminus. The C-terminal region of the protein contains a regulatory domain that is involved in binding other subunits of the complex. It has been shown that β subunits regulate the nuclear and cytoplasmic localization of the Snf1 complex (Vincent et al., 2001), although it is likely that they have other functions that are more poorly characterized. The specific roles of the individual β subunit proteins Sip1, Sip2, and Gal83 are not well understood; however, the presence of at least one β subunit is required for kinase function in vivo (Schmidt and McCartney, 2000), and yeast strains expressing a single β subunit show distinct phenotypes (Nath et al., 2002). Therefore, the three distinct Snf1 complexes formed appear to have specialized roles. The γ subunit is also essential for kinase activity in vivo (Jiang and Carlson, 1997; McCartney, 2001; Schmidt and McCartney, 2000). Previous studies have found that the trimeric Snf1 complex is organized by the binding of the β subunit to both the α and the γ subunits (Jiang and Carlson, 1997; Yang et al., 1994). The γ subunit also binds the regulatory domain of the Snf1 kinase in a glucose-regulated manner (Jiang and Carlson, 1996). Thus, it appears that the β and

*Correspondence: marmor@wistar.org

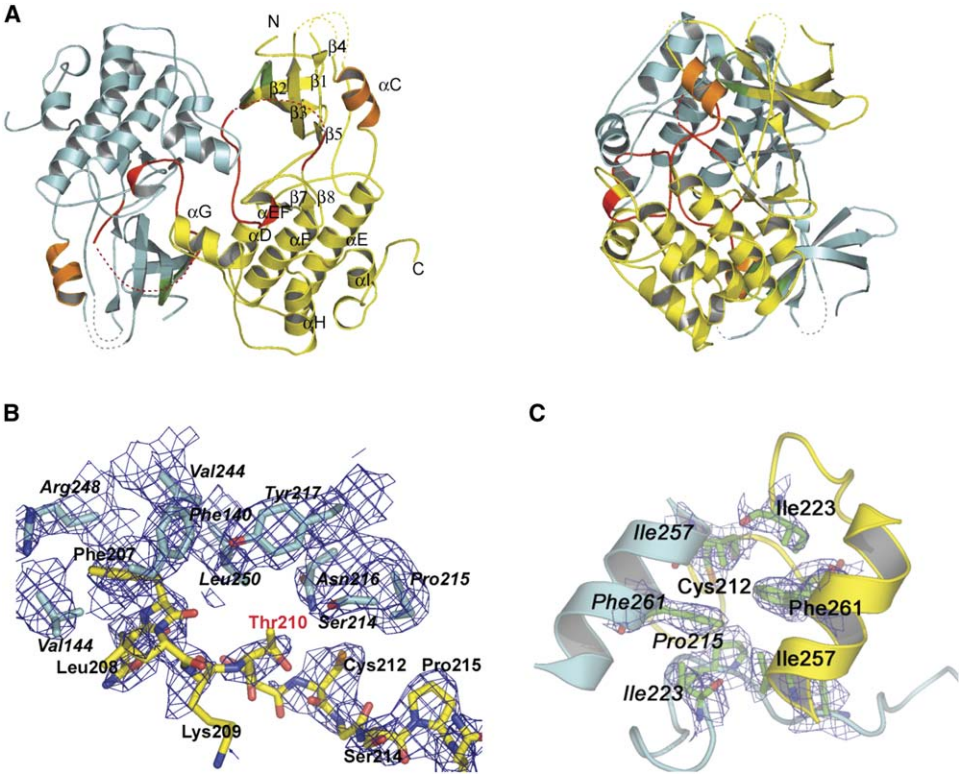

Figure 1. Structure of the Yeast Snf1 Kinase Domain

(A) The Snf1 dimer. The two protomers of the homodimer are shown in yellow and cyan. The ATP binding P loop (green), αC helix (orange), and activation segment T loop (red) are each color coded, and disordered loops are indicated with dotted lines. Secondary structure notation is based on the structure of PKA (Knighton et al., 1991). The image on the right is rotated by about 90° about a vertical axis between the two protomers.

(B) Electron density of the activation segment at the dimerization interface. Activation loop residues of one protomer are colored yellow, and residues from the opposing protomer are colored cyan and labeled in italics. For clarity, only side chain atoms from the opposing protomer are shown. Electron density from a composite omit map is contoured at 0.8σ.

(C) Electron density of the αG helix at the dimerization interface. The image is centered around residues I257 and F261. The color coding and contour level is as described in Figure 1B.

γ subunits regulate Snf1 kinase activity and also confer substrate specificity.

In this study, we report the X-ray crystal structure of the kinase domain of Snf1. The Snf1 kinase domain reveals a typical bilobe kinase fold, with the greatest structural similarity to cyclin-dependant kinase-2. In addition, the crystals reveal a novel homodimeric structure that we show also forms in solution and in yeast cells. Based on sequence conservation, Snf1 dimerization appears to be a conserved feature of the Snf1/AMPK family kinases. Several structural features suggest that this dimer represents an inactive form of the kinases and thus another layer of regulation of the Snf1/AMPK kinases.

Results

Overall Structure of the Snf1 Kinase Domain

The 33 kDa Snf1 kinase domain (residues 33–320) was overexpressed in bacteria and purified to homogeneity using a combination of cation exchange and gel filtration chromatography, where the protein eluted between the 44 and 158 kDa molecular weight standards on a Superdex-75 column, suggestive of a protein dimer. The protein crystallized in space group $P42_12$ containing one molecule per asymmetric unit cell and, consistent with the gel filtration data, the crystals contain a crystallographically related dimer containing 3000 Å^2 of solvent excluded surface at the dimer interface (Figure 1A). The structure was determined to 2.8 Å resolution using multiple wavelength anomalous diffraction (MAD) from selenomethionine-derivatized protein (Table 1).

The kinase domain adopts an elongated bilobe structure that is typical of all kinases. A smaller β-rich N-terminal lobe contains the β3 strand and helix αC harboring the conserved phosphate binding residues Lys84 and Glu103, respectively, and the ATP binding P loop (residues 61–69); and a larger helical-rich C-terminal lobe contains the catalytic Asp177 residue (Figures 1A and 2). The active site, containing the majority of the ATP binding residues and the T loop activation segment (Figure 1B), is located in a groove formed between the two lobes. The two subunits of the crystallographic dimer cross at a roughly 45° angle, with the N-terminal lobe of one subunit proximal to the C-terminal lobe of an opposing subunit, and the dimer interface formed by Snf1/AMPK conserved hydrophobic residues and residues within the T loop activation segment (residues 195–221) from both protomers (Figures 1A–1C).

Table 1. Data Collection, Phasing, and Refinement

Crystal parameters				
Space group $P42_12$				
Unit cell (native)	a = b = 108.67, c = 61.50			
Data collection	Peak	Inflection	Remote	Native
Wavelength (Å)	0.97940	0.97959	0.96863	0.97959
Resolution (Å)	50–3.0	50–3.0	50–3.0	50–2.8
Total reflections	499,502	507,113	513,519	378,898
Unique reflections	7,774	7,778	14,080	11,830
Completeness (%)[a]	100 (100)	100 (100)	100 (100)	99.8 (100)
Avg. I/σ	42.5 (7.6)	36.97 (5.8)	31.5 (5.17)	34.3 (4.3)
R_{merge} (%)[b]	10.3 (48.5)	10.1 (63.3)	8.6 (49.9)	7.1 (52.4)
Refinement statistics				
Resolution range, Å	50–2.8			
$R_{(working)}$, %	22.3			
$R_{(free)}$, %	26.5			
Rmsds from ideal				
Bond lengths (Å)	0.007			
Bond angles (°)	1.374			
	$B_{average}$ (Å^2)	No. of atoms		
Protein	52.27	2057		
Water	49.51	105		

[a] Values in parenthesis are from the highest resolution shell.
[b] $R_{merge} = \sum|I - \langle I\rangle|/\sum\langle I\rangle$.

Comparison with Other Kinases

A comparison of the Snf1 kinase with other protein kinases shows the greatest structural superposition with cyclin-dependent kinase-2 (CDK2) (Figure 3A), with an rmsd between Cα atoms of 1.7 Å. CDK2 is inactive on its own, but is activated upon binding to a cyclin protein.

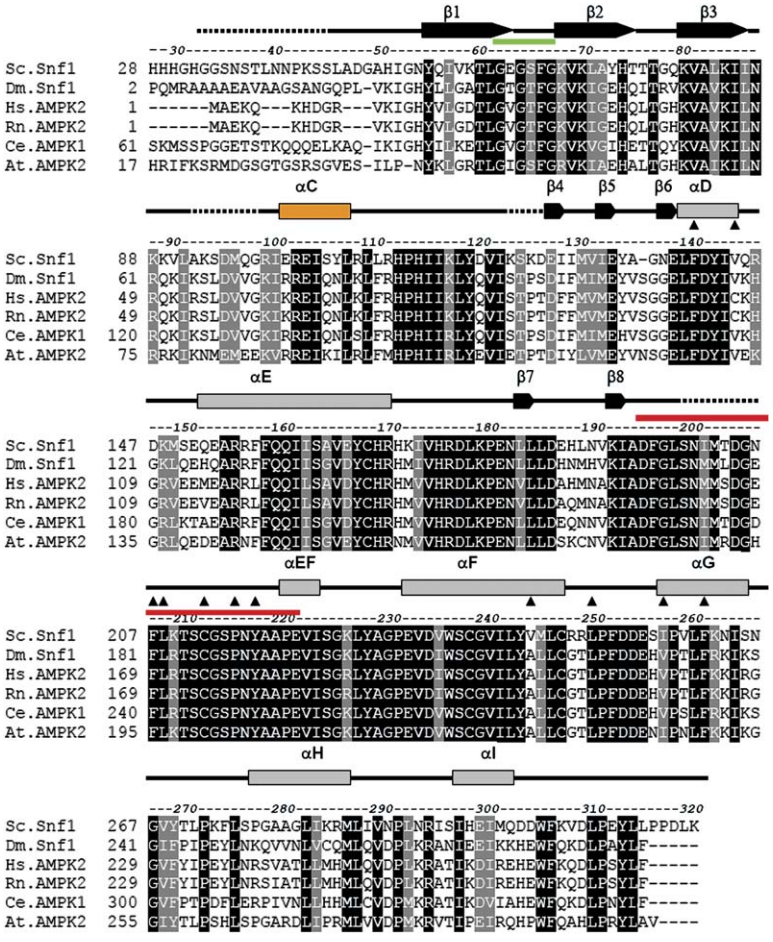

Figure 2. Sequence Alignment of Snf1/AMPK Kinases

Sequences from yeast (Sc: *S. cerevisiae*), fly (Dm = *Drosophila melanogaster*), human (Hs = *Homo sapiens*), rat (Rn = *Rattus norvegicus*), worm (Ce = *Caenorhabditis elegans*) and plant (At = *Arabidopsis thaliana*) were aligned. Snf1 residue numbers are shown at intervals of 10, and Snf1 secondary structure elements are indicated above the alignment. The P loop sequence is denoted by a green bar and the activation T loop sequence by a red bar. Residues involved in the dimerization interface are denoted by triangles above the alignment.

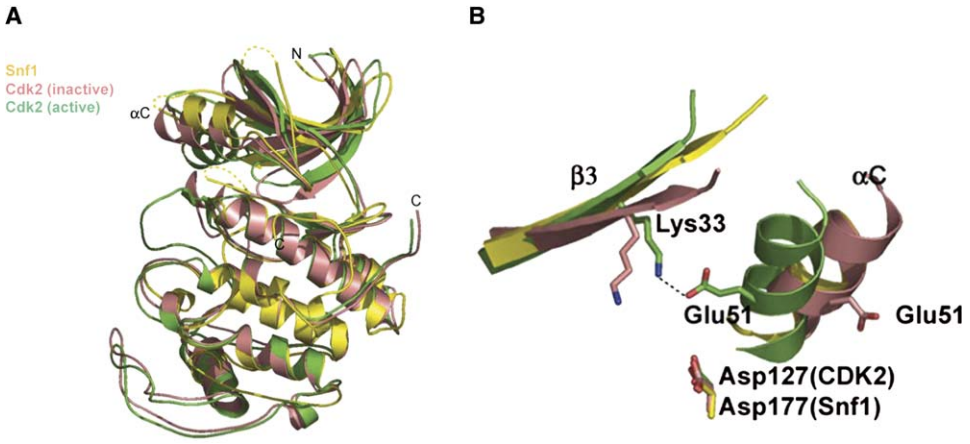

Figure 3. Comparison of Snf1 and CDK2 Kinase Domains

(A) Overall superposition of nascent Snf1, nascent CDK2 and cyclin-bound CDK2 structures.

(B) Close-up view of interactions mediated by αC helix. Cyclin A binding induces a conformation change in the αC helix, leading to the formation of the Lys33-Glu51 hydrogen bond that is associated with CDK2 activation.

The crystal structures of both the inactive and a cyclin A bound active form of the CDK2 kinase have been previously determined (De Bondt et al., 1993; Jeffrey et al., 1995). Of particular interest is the conformation of the conserved αC helix in the N-terminal lobe that adopts two different orientations, dependent on the activation state of the kinase. In active CDK2, the bound cyclin molecule interacts with the αC helix and positions it close to the active site such that a conserved glutamate residue (Glu51 in CDK2) is oriented to form a hydrogen bond with a conserved lysine residue (Lys33 in CDK2) within the β3 strand, which in turn enables the kinase to bind ATP (Figure 3B). In the inactive cyclin-free form, the αC helix of CDK2 is rotated away from the active site such that Glu51 and Lys33 cannot hydrogen bond, thus destabilizing ATP binding, rendering the kinase inactive. In the Snf1 kinase, the corresponding ATP binding residues are Glu103 and Lys84. A superposition of the CDK2 and Snf1 kinase domains reveals that the αC helix containing Glu103 has a conformation that closely resembles the inactive form of CDK2 (Figures 3A and 3B). In addition, the Lys 84 and Glu103 side chains in Snf1 are disordered. This correlation suggests that the Snf1 kinase domain monomer structure that we have determined is in the inactive form.

Interestingly, while all kinases show a comparable Lys-Glu hydrogen bonding network in the active form of the corresponding kinase, the activity of other kinases is also regulated, in part through the allosteric modulation of the αC helix orientation. For example, the αC helix of the Src tyrosine kinase is held in an inactive conformation by intramolecular interactions with the SH2 and SH3 domains, and the phosphorylation-dependent disengagement of these domains from the kinase domain results in a reorientation of the αC helix into an active conformation (Huse and Kuriyan, 2002). Based on these correlations and the observation that the Snf1 kinase requires association with its β and γ subunits for in vivo activity (Sanz, 2003; Schmidt and McCartney, 2000), we propose that one of the roles of one or more of these subunits may be to reorient the αC helix into an active conformation.

The Dimer Interface

As noted above, the crystal structure of the Snf1 kinase reveals a crystallographic dimer containing an extensive dimerization interface (Figures 1A and 1C). This dimerization interface buries a total solvent-excluded surface of 1500 Å^2, and a Lawrence and Colman goodness of fit calculation gives a value of 0.575 (Lawrence and Colman, 1993), both indicative of a significant dimer interface. The physiological relevance of this interface is supported by the observation that the most highly conserved region of the Snf1/AMPK family maps to this interface (Figures 2 and 4A). The dimer interface is formed predominately by hydrophobic interactions involving residues within the T loop activation segment and the loop-αG region of the kinase domain. The T loop activation segment-mediated interactions are centered around Thr210, the target of upstream Snf1 activating kinases, and involve the flanking residues Phe 207, Ile 208, Cys 212, and Pro 215 (Figure 4B). The methyl group of Thr 210 makes van der Waals contacts to the Leu 250 side chain of the symmetry-related Snf1 subunit of the dimer. In addition, residues Phe 207 and Ile 208 make van der Waals contacts to the aliphatic arm of Arg 248 and the Phe 140, Val 144, and Val 244 side chains of the Snf1 symmetry-related subunit; and residues Cys 212 and Pro 215 make van der Waals interactions with the symmetry-related Snf1 side chains Pro215, Ile 250, and Ile 257. The loop-αG interactions centered around Ile 257 and Phe 261 mediate van der Waals contacts to the same residues of the symmetry-related Snf1 subunit of the dimer, and also include the symmetry-related residues Pro 215, Ile 223, and Cys 212 (Figure 4C). Strikingly, nearly all of the residues that mediate dimer interactions are highly conserved within the Snf1/AMPK family (Figure 2), thus implicating the functional importance of the crystallographically observed dimer within the Snf1/AMPK protein family.

A striking feature of the Snf1 dimer observed in the crystals is that Thr 210 is highly buried and inaccessible for phosphorylation by an activating upstream kinase (Figures 1A, 1B, and 4A). In addition, a modeling of ATP and protein peptide substrate onto the Snf1 structure

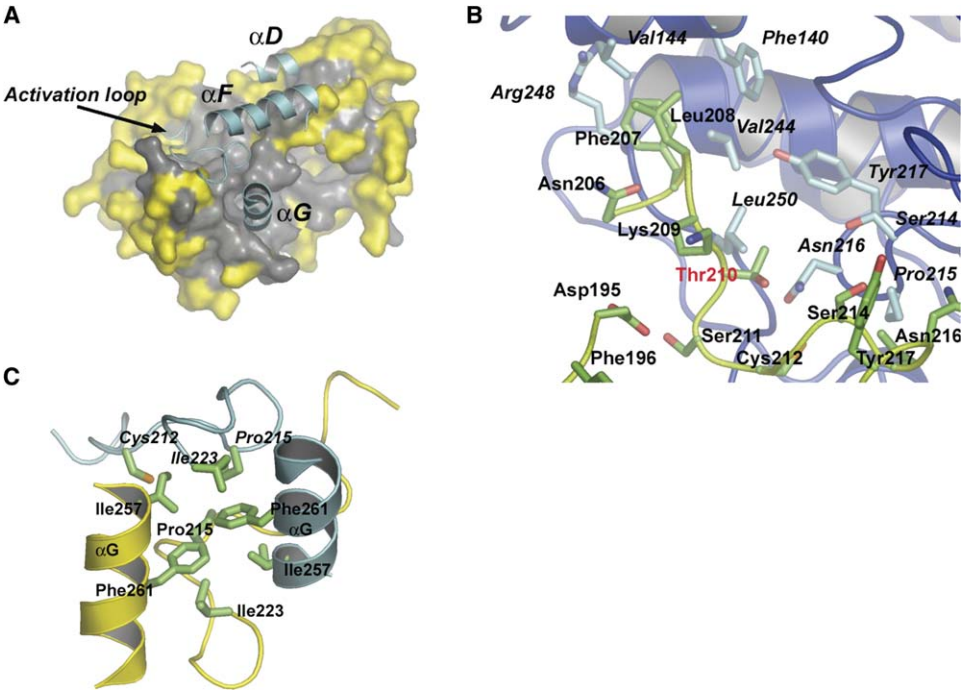

Figure 4. The Crystallographic Snf1 Dimer

(A) Mapping of strictly conserved Snf1/AMPK residues (gray) onto the molecular surface of the kinase domain monomer. Side chain residues that mediate dimer interactions are highlighted in green, and the αG helix and activation segment from the opposing protomer are included in blue schematic with green side chains. The residues from the opposing subunit of the dimer that play key roles in dimer formation are also highlighted as green side chains.

(B) Close-up of the burial of the activation loop residue T210 within the Snf1 kinase domain dimer. The activation loop of one protomer is shown in yellow with side chains in green. Secondary structure elements of the opposing protomer are shown in blue and side chains in cyan are labeled in italics.

(C) Close-up view of dimer interactions mediated by the αG helix and activation segment.

based on a superposition of Snf1 with a CDK2/ATP/protein peptide complex also suggests that the dimer is not compatible with cosubstrate binding. Specifically, while ATP can be modeled onto Snf1 without steric clash, the peptide substrate would make a direct clash with residues 210–212 of the activation segment from the other protomer of the dimer (Figure 5). Taken together, these observations support the hypothesis that the crystallographically observed Snf1 dimer represents an inactive form of the kinase.

Oligomerization State of the Snf1 Kinase Domain in Solution

The crystallographic Snf1 dimer is consistent with its elution on gel filtration chromatography between the 44 and 158 kDa protein standards (Figure 6B). In order to obtain a more definitive and quantitative characterization of the solution oligomerization properties of the Snf1 kinase domain, we performed equilibrium ultracentrifugation of the recombinant kinase domain (Figure 6A). This analysis was carried out at three different centrifugation speeds and three different protein concentrations. Global analysis of these data reveals an excellent fit for a homodimer, with no detectable dissociation to a monomer under the conditions used. These data are consistent with the gel filtration and crystallographic data. To further validate the biological significance of the specific Snf1 dimer seen in the crystals, we prepared two site-directed mutations predicted from the crystallographic dimer to disrupt dimer contacts and analyzed these mutants by gel filtration analysis. The Snf1 positions that were chosen for mutagenesis were Ile 257 and Phe 261, two key hydrophobic residues that stabilize the crystallographic Snf1 kinase domain dimer (Figure 4). These positions were mutated to glutamate residues (I257E and F261E) in an attempt to disrupt this hydrophobic core of the dimer interface. Each of these mutants were prepared by site-directed mutagenesis and purified essentially as described for the native recombinant protein, and then analyzed by gel filtration chromatography. As shown in Figure 6B, the F261E Snf1 mutant elutes as two peaks from gel filtration, corresponding to a monomeric and dimeric Snf1 species, and I257E elutes almost exclusively at a position corresponding to an Snf1 monomer. Taken together, the solution studies on the Snf1 kinase domain show that, as in the crystals, the kinase domain forms a tight dimer. Moreover, the mutational sensitivity of the I257E and F261 for dimer formation is consistent with the physiological relevance of the crystallographic Snf1 dimer.

Self-Association of Full-Length Snf1 in Yeast Cells

In order to probe in vivo self-association of Snf1 molecules, we carried out coimmunoprecipitation experiments in yeast cells. For these experiments, we prepared a yeast strain harboring two alternatively tagged

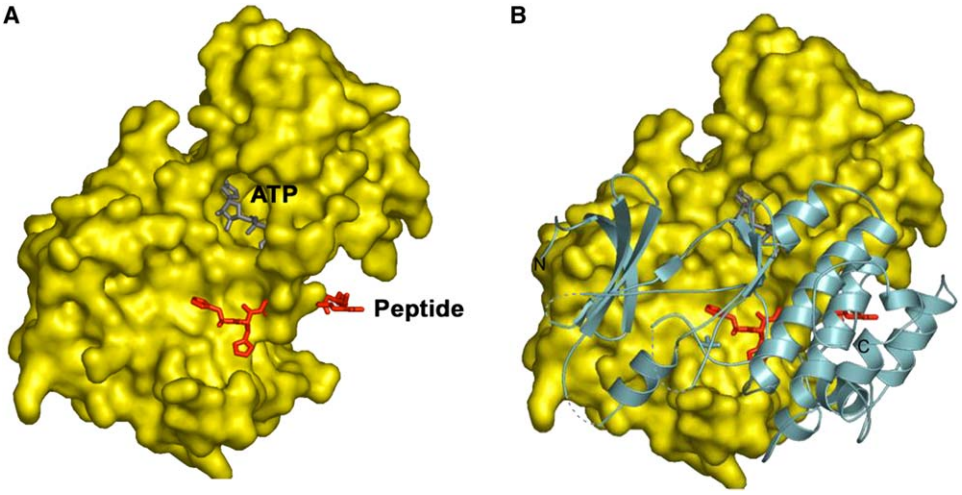

Figure 5. Model for Snf1 Interaction with ATP and Protein Peptide Substrates

(A) Model of Snf1 kinase domain with ATP and substrate peptide superimposed from the crystal structure of active CDK2 with substrate (Brown et al., 1999). The placement of the ATP and peptide substrates is based on the superposition of the kinase domains. The ATP is shown in gray and peptide is shown in red.

(B) The opposing subunit (schematic in cyan) of the Snf1 kinase domain dimer is mapped onto the model in (A) to illustrate the occlusion of the peptide substrate binding site within the Snf1 kinase domain dimer.

(HA and FLAG) full-length Snf1 proteins encoded on separate plasmids, grew the yeast strain, disrupted the cells, and probed for self association using coimmunprecipitation. Immunoprecipitation was carried out with anti-FLAG antibody, and immunoprecipitates were extensively washed, followed by protein separation on SDS-PAGE gels and detection by Western blotting using either anti-HA or anti-FLAG antibodies. As can be seen in Figure 6C, bands corresponding to HA-Snf1 and FLAG-Snf1 were detected with about equal intensity. Similar results were obtained when anti-FLAG precipitates were washed with 50–400 mM NaCl, or if protein was first immunoprecipitated with anti-HA and then blotted with anti-FLAG (Figure 6C). Together, these experiments show that intact Snf1 protein self-associates in vivo, consistent with our in vitro solution studies and crystallographic observation of a dimer of the Snf1 kinase domain.

Interestingly, similar coimmunoprecipitation experiments employing yeast strains encoding HA- and FLAG-tagged mutants that disrupt dimerization of the Snf1 kinase domain when assayed in vitro (I257E and F261E), as well as a K84R control mutant in the Snf1 active site away from the dimerization interface, do not show a significant disruption of Snf1 self-association in vivo (Figure 6C), suggesting that the I257E and F261E mutations are not sufficient to disrupt Snf1 self-association in vivo. These results suggest that other regions of intact Snf1, or possibly other subunits of the heterotrimeric Snf1 complex that forms in vivo, may also contribute to Snf1 self-association in vivo.

Discussion

We have presented the structure of the kinase domain from yeast Snf1, a member of the Snf1/AMPK family of kinases. The high degree of sequence conservation among this family of kinases suggests that they have highly homologous structure, and the structure presented here is thus representative of the kinase family. The structure of the monomeric unit adopts an αC helix conformation that is representative of inactive kinases. A novel feature of the Snf1 kinase domain, both in the crystals and in solution, is that it adopts a dimeric structure that has not been seen in other kinases. There are several reasons to believe that this dimeric Snf1 structure represents an inactive form of the kinase: (1) Thr210, a residue within the activation segment that requires phosphorylation for kinase activation, is buried within the dimer interface, making it inaccessible for phosphorylation by an upstream activating kinase; (2) while ATP can be modeled onto the Snf1 without steric clash, the modeling of peptide substrate reveals that it makes a steric clash with the activation segment of the kinase. Based on these observations, we propose that activation of the Snf1 kinase involves the disruption or rearrangement of the dimer. Together, there appears to be three layers of regulation of Snf1/AMPK activation. First, association must occur with the β and γ subunits, the kinase domain dimer must be destabilized, and Thr 210 within the activation segment must be phosphorylated. It is not clear what may trigger kinase dimer domain destabilization, but it is attractive to propose that either the β or γ subunit or another region of Snf1 itself may do this, perhaps in a way similar to that in which cyclins activate CDK (Pavletich, 1999), or how phosphorylation of the C-terminal tail region of the Src kinase displaces the SH2 and SH3 domains in Src activation (Huse and Kuriyan, 2002). Regardless of the detailed mechanism, it would appear that some form of allosteric regulation must take place in Snf1/AMPK activation and that Snf1/AMPK kinase domain activation involves an additional layer of regulation that is distinct from other kinases.

The observation of coimmunoprecipitation of full-length Snf1 from yeast cells is consistent with dimerization of the kinase domain within the Snf1 protein in vivo. Interestingly, while the F261E and I257E mutants disrupt

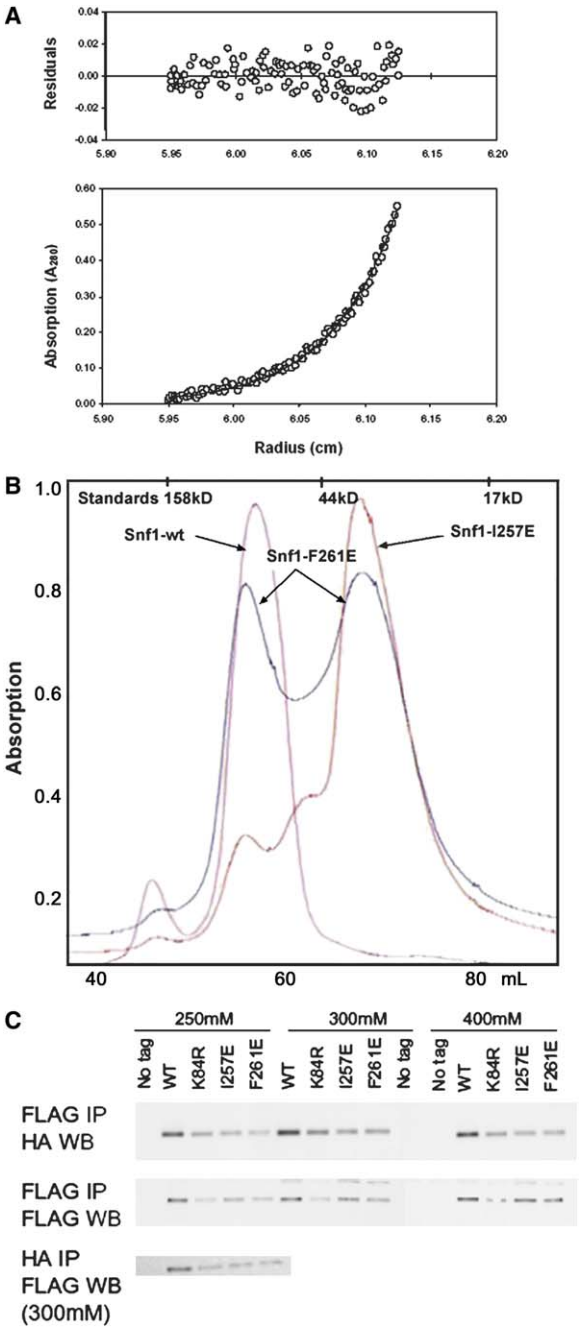

Figure 6. Oligomerization Properties of the Snf1 Kinase Domain

(A) Sedimentation equilibrium data for the native Snf1 kinase domain fitted with data from nine curves (three protein concentrations at three centrifugation speeds). A representative run at a centrifugation speed of 16,000 rpm and protein concentration of 0.3 mg ml^{-1} is shown. The plots represent a single dimeric species model for which all nine curves were fitted. The bottom panel shows the experimental data (open circles) with the calculated fits (lines). The top panel represents the residuals of the fits.

(B) Size exclusion chromatography of native Snf1 and Snf1 mutants I257E and F261E. Each of the proteins is chromatographed on Superdex-75 at a concentration of about 15 mg/ml, and protein elution peaks were identified by UV absorption at 280 nm.

(C) Snf1 coimmunoprecipitation experiments from yeast cells encoding HA- and Flag-tagged full-length Snf1. The antibodies used for the immunoprecipitation and Western blotting are indicated, as well as the salt wash used for washing the immunoprecipitate prior to Western analysis.

dimerization of the kinase domain in vitro, our coimmunoprecipitation experiments reveal that these mutations are not sufficient to disrupt Snf1 self-association in vivo. This observation suggests that the Snf1-Snf1 association may involve more than the Snf1 kinase domain interface observed in the crystal structure. This interface could involve regions of Snf1 outside the kinase domain, such as the regulatory domain, and/or the β or γ subunits of the Snf1 complex.

Mammalian Pak1 represents another structurally characterized kinase that forms a homodimer. Like Snf1, the Pak1 homodimer forms an autoinhibited complex, although the mode of autoinhibition appears distinct from Snf1. The structure of Pak1 reveals a trans-inhibited homodimeric conformation, in which an N-terminal inhibitory portion of one protomer binds to and inhibits the catalytic domain of the other protomer, and associated biochemical studies reveal that GTPase interaction disrupts dimer formation and facilitates activation of the kinase (Parrini et al., 2002). Interestingly, there are many more examples of kinases that contain *cis* autoinhibitory domains. Although it is not clear if there is a distinction between kinases that form autoinhibitory complexes in *cis* or in *trans* that might have particular biological ramifications, *trans* inhibition would be expected to introduce another layer of kinase regulation that involves protein oligomerization that might be exploited in vivo. Regardless of the mechanism of kinase autoinhibition, it appears that there exists a greater diversity for kinase inhibition than for kinase activation, and that this diversity might be exploited for the design of kinase-specific regulatory compounds.

Because of the correlation between AMPK kinase activity and several human disorders, including type II diabetes, obesity, cardiac disease, and cancer, and the observation that pharmacological factors that are beneficial in these disorders have been shown to act, at least in part, through the activation of AMPK (Arad et al., 2002; Minokoshi et al., 2002; Woods et al., 2003; Zhou et al., 2001), there has been significant interest in the development of small-molecule AMPK activators that might have therapeutic application (Clapham, 2004). Although there are several kinase-specific inhibitors that have been developed for therapeutic purposes, the development of kinase-specific activators are technically more challenging (Noble et al., 2004). Our structural findings on the Snf1/AMPK kinase domain suggest a strategy for developing Snf1/AMPK activators that takes advantage of the unique dimerization properties of these kinases. Compounds that inhibit kinase domain dimerization may thus relieve one layer of AMPK regulation, thus facilitating AMPK-specific activation in AMPK-mediated human disorders.

Experimental Procedures

Protein Overexpression and Purification

The wild-type kinase domain of Snf1 (residues 33–320) was cloned into the pRSET overexpression vector with an upstream 15 base pair insert encoding a MKAAA N-terminal sequence to enhance protein expression. The cloned kinase domain was expressed in BL21 (DE3) cells by induction with 0.5 mM IPTG at 15ºC. The protein was purified using SP-sepharose cation exchange chromatography followed by size-exclusion chromatography on a Superdex-75 gel filtration column. Peak fractions from the gel filtration column were

pooled and concentrated to ~30 mg/ml by ultracentrifugation with a Millipore microconcentrator, flash frozen, and stored at −70ºC until further use. Selenomethionine-derivatized protein was expressed in B834 (DE3) cells grown in MOPS minimal media with selenomethionine and other amino acids at suggested concentrations (Doublie, 1997). Purification of the selenomethionine-derivatized protein was carried out essentially as described for the underivatized protein. The single amino acid substitution mutants Snf1-I257E and Snf1-F261E were prepared by site-directed mutagenesis (QuikChange, Stratagene) and purified essentially as described for the wild-type kinase domain.

Crystallization and Data Collection

Snf1 kinase domain crystals were obtained by vapor diffusion using the hanging drop method. A 2 μl aliquot of the protein solution at 10 mg/ml in a buffer containing 20 mM HEPES, 100 mM NaCl, 10 mM β-mercaptoethanol was mixed with 2 μl of reservoir solution containing 0.1 M Tris (pH 8.5), 0.2 M $MgCl_2$, 24%–30% polyethylene glycol 4000, and equilibrated over 500 μl of reservoir solution at room temperature. The crystals grew over 3–4 days, and native and selenomethionine-derivatized crystals grew to typical sizes of 400 × 400 × 50–100 μm and 100 × 100 × 50 μm, respectively. Crystals were cryoprotected by transferring them into reservoir solution supplemented with increasing amounts of glycerol to a final concentration of 15% and flash frozen in liquid propane, at which point they were stored in liquid nitrogen until data collection.

To remove possible artifacts from model bias, we determined the structure of the Snf1 kinase domain using MAD rather than molecular replacement with other kinase domains as search models. Data from native and selenomethionine crystals were collected at beamline SBC-19BM at the Advanced Photon Source, Argonne National Laboratory. The native data was collected at λ = 0.9696 Å and produced useable diffraction data to 2.8 Å resolution. A 3.0 Å MAD data set was collected from a single selenomethionine-derivatized crystal at three wavelengths (λ1 = 0.9794 Å, peak; λ2 = 0.9796 Å, edge; λ3 = 0.9686 Å, remote). All data were processed with DENZO and SCALEPACK, and the space group was determined to be $P42_12$.

Structure Determination and Refinement

The structure of the Snf1 kinase domain was solved by MAD. The program SOLVE was used to located five selenomethionine residues and to phase the 3.0 Å electron density map. The map was improved by solvent flattening using the program RESOLVE, and the program O was used to build a molecular model of the protein into the electron density map using the selenomethionine positions as a guide. The native data set was used to extend the resolution to 2.8 Å, and refinement employed the program CNS, using simulated annealing and torsion angle dynamics protocols with subsequent manual adjustment of the model, with reference to $2F_o$-Fc, and difference maps, using the program O. Water molecules that showed appropriate 2 σ density peaks in Fo-Fc maps and that participated in hydrogen bonds with protein residues or other water molecules were added after the free R value dropped below 30%, and, toward the end of refinement, atomic B-factors were refined. The final model was checked for errors using composite simulated annealing maps. The final model contains residues 46–319. Residues 90–97, 123–126 and 199–205 were not modeled due to poor electron density corresponding to these regions. The final model has excellent refinement statistics and stereochemical parameters (Table 1).

Analytical Ultracentrifugation and Gel Filtration Analysis

Sedimentation equilibrium experiments were performed with a Beckman Optima XL1 ultracentrifuge at 4ºC, and in a buffer containing 20 mM HEPES, 100 mM NaCl, and 1 mM β-mercaptoethanol. The protein samples were loaded in 6 sector 12 mm centerpieces. The native Snf1 kinase domain samples were analyzed at concentrations of 0.15, 0.30, and 0.60 mg/ml, and each protein concentration was analyzed at centrifugation speeds of 16,000, 20,000, and 24,000 rpm. Samples were detected using absorption optics at 280 nm, and equilibrium was assessed by comparing successive scans using the MATCH program. Raw data were edited using the REEDIT program, and data analysis was carried out using the NONLIN program. Global data fits were carried out to calculate the effective molecular weight in an ideal single-species model. Models for associating molecules used the calculated σ values from the monomer molecular weight and fitted to dissociation constants. The quality of the fits was assessed by examining residuals and minimizing the fit variance.

Coimmunoprecipitation of Snf1

The yeast strains prepared for coimmunoprecipitation experiments were as follows:

No tag (YMFS182): *MATa ura3 leu2*-3,112 *his3*-11,15 *trp1*-1 *ade2*-1 *can1*-100 snf1::*his5*+ [pRS316] [pRS315]
Snf1 Wild-type (YMFS183): *MATa ura3 leu2*-3,112 *his3*-11, 15 *trp1*-1 *ade2*-1 *can1*-100 *snf1*::*his5*+ [pRS316 *SNF1*-2×FLAG] [pRS315 *SNF1*-2×HA]
Snf1 K84R (YMFS185): *MATa ura3 leu2*-3,112 *his3*-11, 15 *trp1*-1 *ade2*-1 *can1*-100 *snf1*::*his5*+ [pRS316 *snf1*K84R-2×FLAG] [pRS315 *snf1*K84R-2×HA]
Snf1 I257E (YMFS193): *MATa ura3 leu2*-3,112 *his3*-11, 15 *trp1*-1 *ade2*-1 *can1*-100 *snf1*::*his5*+ [pRS316 *snf1*I257E-2×FLAG] [pRS315 *snf1*I257E-2×HA]
Snf1 F261E (YMFS195): *MATa ura3 leu2*-3,112 *his3*-11, 15 *trp1*-1 *ade2*-1 *can1*-100 *snf1*::*his5*+ [pRS316 *snf1*F261E-2×FLAG] [pRS315 *snf1*F261E-2×HA]

Strains containing two alternatively tagged versions of wild-type or mutant *SNF1* on separate plasmids (*SNF1*-2×HA and *SNF1*-2×FLAG) were grown in SC-uracil-leucine media to mid-log phase. Cells were then harvested and resuspended in lysis buffer (50 mM $NaPO_4$ [pH 7.2], 50–400 mM NaCl, 1 mM EDTA, 10% glycerol, 0.1% Triton X-100, 10 mM NaF, 10 mM β-glycerophosphate, 1 mM 1,10-phenanthroline, 1 mM PMSF, Complete Mini, EDTA-free protease inhibitor cocktail tablets [Roche]), and lysis was performed by mechanical disruption using a Mini-beadbeater (Biospec). Lysates were then clarified by centrifugation, and equal amounts of protein from each strain were immunoprecipitated with anti-FLAG (M2) or anti-HA (HA-7) agarose (Sigma). Bound proteins were washed (with lysis buffer containing the same NaCl concentration used for lysis) and eluted by boiling in SDS-PAGE sample buffer. Eluted proteins were run on 10% SDS-PAGE gels and transferred to nitrocellulose for Western analysis. Western blotting was performed with anti-FLAG (M2) HRP conjugate (Sigma) or anti-HA (3F10) HRP conjugate (Roche) antibodies, following the manufacturer's recommendations.

Acknowledgments

The authors wish to thank A. Joachimiak and N. Duke and the SBC-CAT staff for access to and assistance with the 19BM beamline for data collection at Argonne National Laboratories, and David Speicher and Sandra Harper for assistance using the Beckman Optima XL-1 analytical centrifuge. This work was supported by an NIH grant to R.M. and by a grant from the Commonwealth Universal Research Enhancement Program, Pennsylvania Department of Health, awarded to the Wistar Institute.

Received: June 15, 2005
Revised: December 14, 2005
Accepted: December 15, 2005
Published online: March 14, 2006

References

Arad, M., Benson, D.W., Perez-Atayde, A.R., McKenna, W.J., Sparks, E.A., Kanter, R.J., McGarry, K., Seidman, J.G., and Seidman, C.E. (2002). Constitutively active AMP kinase mutations cause glycogen storage disease mimicking hypertrophic cardiomyopathy. J. Clin. Invest. *109*, 357–362.

Ausio, J., Abbott, D.W., Wang, X., and Moore, S.C. (2001). Histone variants and histone modifications: a structural perspective. Biochem. Cell Biol. *79*, 693–708.

Brown, N.R., Noble, M.E., Endicott, J.A., and Johnson, L.N. (1999). The structural basis for specificity of substrate and recruitment peptides for cyclin-dependent kinases. Nat. Cell Biol. *1*, 438–443.

Carling, D. (2004). The AMP-activated protein kinase cascade: a unifying system for energy control. Trends Biochem. Sci. *29*, 18–24.

Clapham, J.C. (2004). Treating obesity: pharmacology of energy expenditure. Curr. Drug Targets *5*, 309–323.

De Bondt, H.L., Rosenblatt, J., Jancarik, J., Jones, H.D., Morgan, D.O., and Kim, S.H. (1993). Crystal structure of cyclin-dependent kinase 2. Nature *363*, 595–602.

Doublie, S. (1997). Preparation of selenomethionyl proteins for phase determination. In Methods in Enzymology: Macromolecular Crystallography, Part A, C.W. Carter, and R.M. Sweet, eds. (New York, N.Y.: Academic Press, Inc.), pp. 523–530.

Grant, P.A. (2001). A tale of histone modifications. Genome Biol. *2*, REVIEWS0003. Published online April 5, 2005.

Halford, N.G., Hey, S., Jhurreea, D., Laurie, S., McKibbin, R.S., Zhang, Y., and Paul, M.J. (2004). Highly conserved protein kinases involved in the regulation of carbon and amino acid metabolism. J. Exp. Bot. *55*, 35–42.

Hardie, D.G., Carling, D., and Carlson, M. (1998). The AMP-activated/SNF1 protein kinase subfamily: metabolic sensors of the eukaryotic cell? Annu. Rev. Biochem. *67*, 821–855.

Hiesinger, M., Roth, S., Meissner, E., and Schuller, H.J. (2001). Contribution of Cat8 and Sip4 to the transcriptional activation of yeast gluconeogenic genes by carbon source-responsive elements. Curr. Genet. *39*, 68–76.

Huse, M., and Kuriyan, J. (2002). The conformational plasticity of protein kinases. Cell *109*, 275–282.

Jeffrey, P.D., Russo, A.A., Polyak, K., Gibbs, E., Hurwitz, J., Massague, J., and Pavletich, N.P. (1995). Mechanism of CDK activation revealed by the structure of a cyclinA-CDK2 complex. Nature *376*, 313–320.

Jiang, R., and Carlson, M. (1996). Glucose regulates protein interactions within the yeast SNF1 protein kinase complex. Genes Dev. *10*, 3105–3115.

Jiang, R., and Carlson, M. (1997). The Snf1 protein kinase and its activating subunit, Snf4, interact with distinct domains of the Sip1/Sip2/Gal83 component in the kinase complex. Mol. Cell. Biol. *17*, 2099–2106.

Knighton, D.R., Zheng, J.H., Ten Eyck, L.F., Xuong, N.H., Taylor, S.S., and Sowadski, J.M. (1991). Structure of a peptide inhibitor bound to the catalytic subunit of cyclic adenosine monophosphate-dependent protein kinase. Science *253*, 414–420.

Kuchin, S., Treich, I., and Carlson, M. (2000). A regulatory shortcut between the Snf1 protein kinase and RNA polymerase II holoenzyme. Proc. Natl. Acad. Sci. USA *97*, 7916–7920.

Lawrence, M.C., and Colman, P.M. (1993). Shape complementarity at protein/protein interfaces. J. Mol. Biol. *234*, 946–950.

Lo, W.S., Duggan, L., Emre, N.C., Belotserkovskya, R., Lane, W.S., Shiekhattar, R., and Berger, S.L. (2001). Snf1: a histone kinase that works in concert with the histone acetyltransferase Gcn5 to regulate transcription. Science *293*, 1142–1146.

Lo, W.S., Gamache, E.R., Henry, K.W., Yang, D., Pillus, L., and Berger, S.L. (2005). Histone H3 phosphorylation can promote TBP recruitment through distinct promoter-specific mechanisms. EMBO J. *24*, 997–1008.

McCartney, R.R. (2001). Regulation of Snf1 kinase: activation requires phosphorylation of threonine 210 by an upstream kinase as well as a distinct step mediated by the Snf4 subunit. J. Biol. Chem. *276*, 36460–36466.

Minokoshi, Y., Kim, Y.B., Peroni, O.D., Fryer, L.G., Muller, C., Carling, D., and Kahn, B.B. (2002). Leptin stimulates fatty-acid oxidation by activating AMP-activated protein kinase. Nature *415*, 339–343.

Nath, N., McCartney, R.R., and Schmidt, M.C. (2002). Purification of characterization of Snf1 kinase complexes containing a defined β subunit composition. J. Biol. Chem. *277*, 50403–50408.

Noble, M.E., Endicott, J.A., and Johnson, L.N. (2004). Protein kinase inhibitors: insights into drug design from structure. Science *303*, 1800–1805.

Parrini, M.C., Lei, M., Harrison, S.C., and Mayer, B.J. (2002). Pak1 kinase homodimers are autoinhibited in trans and dissociated upon activation by Cdc42 and Rac1. Mol. Cell *9*, 73–83.

Pavletich, N.P. (1999). Mechanisms of cyclin-dependent kinase regulation: structures of Cdks, their cyclin activators, and Cip and INK4 inhibitors. J. Mol. Biol. *287*, 821–828.

Sanz, P. (2003). Snf1 protein kinase: a key player in the response to cellular stress in yeast. Biochem. Soc. Trans. *31*, 178–181.

Schmidt, M.C., and McCartney, R.R. (2000). Beta-subunits of Snf1 kinase are required for kinase function and substrate definition. EMBO J. *19*, 4936–4943.

Strahl, B.D., and Allis, C.D. (2000). The language of covalent histone modifications. Nature *403*, 41–45.

Treitel, M.A. (1998). Snf1 protein kinase regulates phosphorylation of the Mig1 repressor in *Saccharomyces cerevisiae*. Mol. Cell. Biol. *18*, 6273–6280.

Vincent, O., Townley, R., Kuchin, S., and Carlson, M. (2001). Subcellular localization of the Snf1 kinase is regulated by specific beta subunits and a novel glucose signaling mechanism. Genes Dev. *15*, 1104–1114.

Woods, A., Johnstone, S.R., Dickerson, K., Leiper, F.C., Fryer, L.G., Neumann, D., Schlattner, U., Wallimann, T., Carlson, M., and Carling, D. (2003). LKB1 is the upstream kinase in the AMP-activated protein kinase cascade. Curr. Biol. *13*, 2004–2008.

Yang, X., Jiang, R., and Carlson, M. (1994). A family of proteins containing a conserved domain that mediates interaction with the yeast SNF1 protein kinase complex. EMBO J. *13*, 5878–5886.

Zhou, G., Myers, R., Li, Y., Chen, Y., Shen, X., Fenyk-Melody, J., Wu, M., Ventre, J., Doebber, T., Fujii, N., et al. (2001). Role of AMP-activated protein kinase in mechanism of metformin action. J. Clin. Invest. *108*, 1167–1174.

Accession Numbers

Coordinates for the Snf1 kinase domain have been deposited in the Rutgers Collaborative Structural Bioinformatics database under accession number 2FH9.